Regular Article

Lanthanum cobaltite perovskite supported on zirconia as an efficient heterogeneous catalyst for activating Oxone in water

Kun-Yi Andrew Lin [a,*], Yu-Chien Chen [a], Tien-Yu Lin [a], Hongta Yang [b,*]

[a] Department of Environmental Engineering, National Chung Hsing University, 250 Kuo-Kuang Road, Taichung, Taiwan
[b] Department of Chemical Engineering, National Chung Hsing University, 250 Kuo-Kuang Road, Taichung, Taiwan

GRAPHICAL ABSTRACT
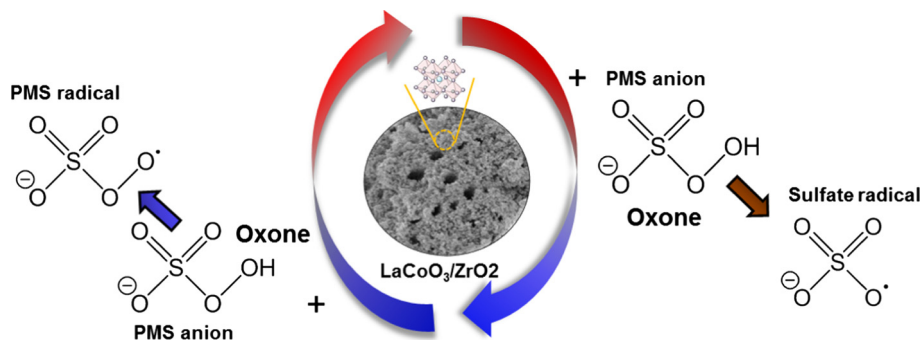
ARTICLE INFO

ABSTRACT

Zirconia-supported $LaCoO_3$ perovskite ($LaCoO_3/ZrO_2$ (LCZ)) is prepared and adopted for the first time as a heterogeneous catalyst for activating Oxone to degrade organic pollutants. The resulting LCZ exhibits a significantly higher surface area (*i.e.*, 10 times) than bulk $LaCoO_3$ powder as nanoscale $LaCoO_3$ particles were easily afforded on the surface of ZrO_2 support. As Rhodamine B (RB) decolorization is selected as a model test to evaluate catalytic activity for activating Oxone, LCZ showed a much higher catalytic activity to activate Oxone than $LaCoO_3$ even though LCZ contained only 12.5 wt% of $LaCoO_3$. LCZ-activated Oxone also remained effective for RB decolorization even in the presence of salts and other organic contaminant. The mechanism of RB decolorization by LCZ-activated Oxone was revealed and involved sulfate radical and other reactive oxygen species. The mechanism of Oxone activation by LCZ could be owing to both La^{3+} and Co^{3+} of LCZ. LCZ was recycled to activate Oxone for RB decolorization over multiple times without loss of catalytic activity. These results demonstrate that LCZ is a promising $LaCoO_3$-based nanocomposite as a heterogeneous catalyst for activating Oxone to degrade organic pollutants.

© 2017 Elsevier Inc. All rights reserved.

1. Introduction

Advanced oxidation processes (AOPs) represent one of the most extensively employed approaches to degrade organic contaminants in wastewater treatments [1]. In AOPs, high-oxidation-potential radicals, such as OH· and SO_4^-, are generated and used to attack organic molecules. To date, many techniques have been intensively developed to generate OH·, for instance, the Fenton's reaction [2]. Nevertheless, processes for obtaining SO_4^- are also attractive owing to the comparable or even higher oxidation potential of SO_4^- than OH· [3]. The SO_4^- also exhibits a high degra-

dation selectivity towards aromatic/unsaturated chemical structures with a relatively short half-life compared to OH· [3].

To obtain SO_4^-, Oxone (*i.e.*, potassium peroxymonosulfate) is the most common source. Nevertheless, the self-decomposition of Oxone is quite slow and thus treatments are required to activate Oxone for generation of SO_4^-. While many treatments have been developed to activate Oxone, including thermal, acoustic, irradiative treatments as well as usage of catalysts, usage of catalysts are much favorable in view of continuous energy consumption by other above-mentioned treatments [4]. Therefore, many non-metallic catalysts (*e.g.*, amorphous boron [5], graphene [6], carbon sphere [7], nitrogen-doped graphene [8,9]) and metal oxides (*e.g.*, cobalt [10], copper [11], iron [12], and manganese oxides [13]) have been proposed to activate Oxone. As metal oxides are proven as useful catalysts for Oxone activation, perovskite-type metal oxides are particularly intriguing and promising as heterogeneous catalysts to activate strong oxidants in AOPs because perovskite-type metal oxides exhibit high stability under aggressive conditions and relatively high degree of stabilization of transition metals in their oxidation states, as well as oxygen mobility within perovskites [14]. These characteristics have enabled perovskites useful catalysts for activating H_2O_2 [14], persulfate [15] and Oxone [16–18]. Nevertheless, the perovskites used in these AOPs are typically bulk powders with relatively low surface areas because perovskite particles tend to pack closely [14], limiting catalytic activities of perovskites. For example, Lanthanum (La)-based perovskites, the most common type of perovskite, exhibit surface areas smaller than 6 $m^2 g^{-1}$ [14]. Even though surface areas of these La-based perovskites can be improved, a complex hard-templating method must be implemented in order to prepare hollow La-based perovskites [19]. Thus, it is still necessary to develop a simple-to-prepare and highly efficient perovskite for activating Oxone. As catalysis primarily involves surface functionalities of catalysts, it is more practical to prepare substrate-supported perovskites. Via immobilizing nanoscale perovskites on porous supports can also increase surface areas of catalysts. Moreover, to our knowledge, this type of supported perovskites has not been investigated for activating Oxone. Thus, in this study, we propose to develop a substrate-supported perovskite as a heterogeneous catalyst for activating Oxone. As La-based perovskites are the most common perovskites, $LaCoO_3$ is selected as a representative La-based perovskite because Co is proven as the most effective metal for activating Oxone [4,20]. To support $LaCoO_3$, zirconia (ZrO_2) is particularly adopted because ZrO_2 remains highly stable under oxidizing and reducing atmospheres, and possesses both acid and base properties, making ZrO_2 as a promising support [21]. While Al_2O_3 is another typical support, Al_2O_3 is shown to react with loaded catalysts, forming new compounds. However, ZrO_2 does not form such compounds; therefore it does not interfere with catalytic processes [21]. A previous study has indicated that ZrO_2 is the most suitable support for perovskites for oxidative reactions in comparison with Al_2O_3 and SiO_2 [22]. ZrO_2 is also shown to be more advantageous than anther common support, TiO_2, because TiO_2 is reducible under the reduced pressure or in the reducing environment. In contrast, ZrO_2 is highly stable under those conditions and even under the photo irradiation [21]. ZrO_2 is also shown to facilitate the formation of nanoscale functionalities on its surface and also to stabilize these resulting nanoparticles, avoiding migration, aggregation and sintering of these nanoparticles during catalytic reactions [23]. Thus, even though ZrO_2 seems more expensive compared to Al_2O_3 and SiO_2, ZrO_2 is still a more promising support for perovskites.

Decolorization of a toxic dye (Rhodamine B (RB)) by sulfate radicals from activation of Oxone by the as-prepared $LaCoO_3/ZrO_2$ (LCZ) is employed as a model test. Activation of Oxone by LCZ under various conditions is examined via investigating different effects on RB decolorization behaviors, including LCZ and Oxone concentrations, temperature, pH, and co-existing compounds. Mechanisms of RB decolorization by LCZ-activated Oxone and activation of Oxone by LCZ are also revealed. Recyclability of LCZ is evaluated to investigate whether LCZ perovskites can be re-used.

2. Experimental

2.1. Preparation and characterization of $LaCoO_3/ZrO_2$ (LCZ)

To prepared $LaCoO_3/ZrO_2$ (LCZ), the porous ZrO_2 support was first synthesized hydrothermally based on literatures [23]. The resulting ZrO_2 powder (1.5 g) was added to 10 mL of glycine solution (1 M) containing equimolar $La(NO_3)_3$ and $Co(NO_3)_2$ (*i.e.*, 0.1 M) [14,24]. The mixture was stirred and maintained at 60 °C for 12 h to yield a sol-like solution, which was subsequently evaporated to remove water and then calcined at 600 °C for 2 h in air to obtain $LaCoO_2/ZrO_2$ (LCZ). $LaCoO_3$ (without ZrO_2 support) was also prepared for comparison using the aforementioned procedure in the absence of ZrO_2.

The as-synthesized perovskites were first characterized by scanning electronic microscopy (SEM) (JEOL JSM-6700, Japan) equipped with Energy-dispersive X-ray spectroscopy (EDS) (Oxford Instrument, UK) for their morphologies. XRD patterns of perovskites were measured using an X-ray diffractometer (Bruker D8 Discover, USA). Surface areas of perovskites were determined using a volumetric gas sorption analyzer (Quantachrome AutoSorb IQ, USA).

2.2. Activation of Oxone by $LaCoO_3/ZrO_2$ (LCZ) perovskite

To evaluate catalytic activity of LCZ for activating Oxone to generate sulfate radicals, decolorization of RB dye by radicals was selected as a model test. In brief, 20 mg of Oxone was first dissolved in 0.2 L of RB solution with an initial concentration (C_0) of 10 mg L^{-1} and then 20 mg of LCZ powder was also added to the RB solution. Sample aliquots were withdrawn from the RB solution at pre-set times and the remaining concentration of RB at a reaction time t (C_t) was measured using an UV–Visible spectrophotometer. Activation behaviors of Oxone by LCZ under different conditions were investigated via examining effects of catalyst/Oxone concentration, temperature (10, 30, 40 and 60 °C), pH (3, 5, 7, 9 and 11), salts (NaF and NaCl), surfactant (sodium dodecyl sulfate (SDS)) and radical quenchers (*i.e.*, ascorbic acid, *tert*-butyl alcohol (TBA) and methanol). Recyclability of perovskites for activating Oxone was tested by using recycled LCZ for decolorization over multiple cycles. The leaching out of metals from LCZ was determined by ICP-OES (Perkin Elmer Optima 8000, USA).

3. Results and discussion

3.1. Characterization of perovskites

As mentioned in the introduction, typical La-based perovskites appear to be non-porous and closely-packed granules with very low surface areas. Thus, the morphology of $LaCoO_3$ is first revealed as a reference in Fig. 1(a). One can note that $LaCoO_3$ particles are a few hundred nanometers and closely-packed, leading to a relatively flat surface. As a result, the surface area is determined merely 6.2 $m^2 g^{-1}$ (Table S1). However, when ZrO_2 support was employed, fine particles of $LaCoO_3$ can be easily afforded on ZrO_2 surface as shown in Fig. 1(b) [23]. Some holes with a size of ~500 nm can be easily noticed on the surface of LCZ, attributed to the porosity of ZrO_2 support. A closer view of LCZ (Fig. 1(c)) displays that the resulting $LaCoO_3$ particles on ZrO_2 support were
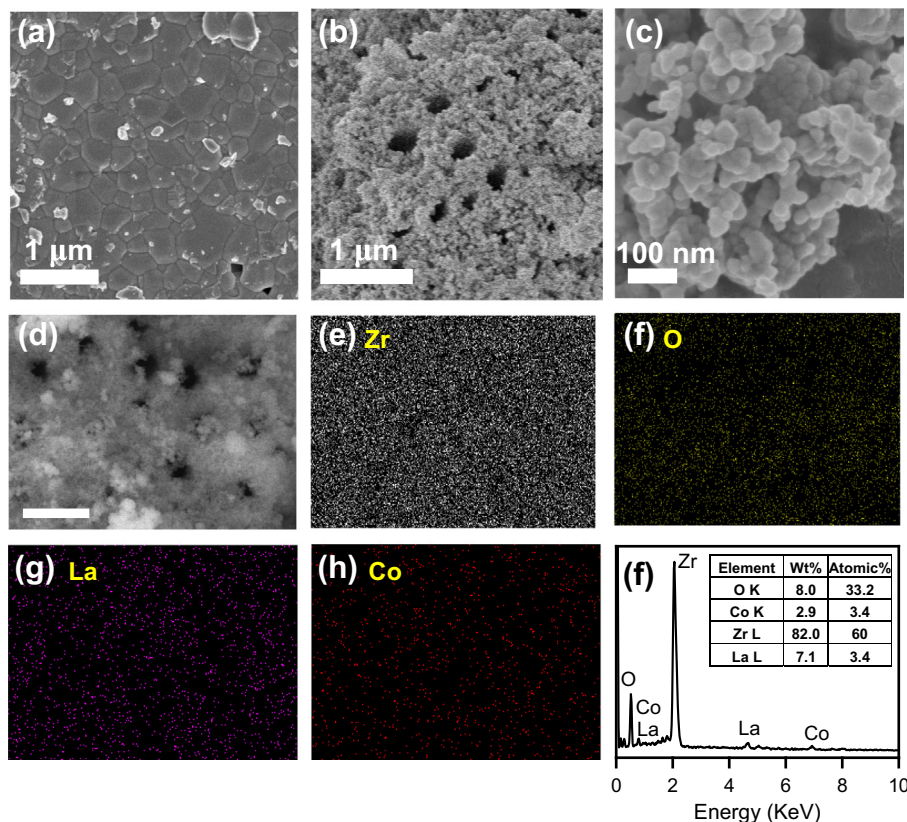
**Fig. 1.** Morphologies of (a) LaCoO₃, (b) and (c) LaCoO₃/ZrO₂ (LCZ) under different magnifications, (d) EDS analysis of LCZ, (e) image of LCZ sample selected for mapping, and (f)–(i) mapping results of constituent elements.

extremely small with sizes of a few ten nanometers. Therefore, LCZ can exhibit a relatively high surface area as 62.5 m² g⁻¹, which is 10 times higher than that of the bulk $LaCoO_3$ powder.

To further ensure the formation of $LaCoO_3$ on ZrO_2 support, an element mapping analysis of LCZ was conducted as shown in Fig. 1(d)–(h). Fig. 1(e) reveals that the area selected in Fig. 1(d) contains a very high concentration of Zr. Fig. 1(f) also reveals a very high concentration of O in LCZ. The presence of Zr and O all over the selected area confirms that the matrix of LCZ was ZrO_2. Fig. 1 (g) and (h) validates the existence of La and Co on the surface of ZrO_2; the concentrations of La and Co are less than Zr and O. The EDS spectrum and chemical composition of LCZ are summarized in Fig. 1(i), showing that fractions of La and Co in LCZ are indeed smaller than ZrO_2. However, La and Co both accounted for 3.4 at. % of LCZ, validating the formation of $LaCoO_3$ on ZrO_2 as La and Co are equimolar. The fraction of $LaCoO_3$ in LCZ can be then estimated as 12.5 wt%.

The formation of $LaCoO_3$ can be also revealed via XRD analyses. Fig. 2 shows XRD patterns of LCZ, $LaCoO_3$ and ZrO_2. The XRD pattern of ZrO_2 displayed in Fig. 2(c) can be readily indexed to the monoclinic ZrO_2 according to JCPDS 37-1484. In addition, the peaks shown in Fig. 2(b) can be indexed to rhombohedral $LaCoO_3$ perovskite (JCPDS 48-0123) [25]. The pattern in Fig. 2(a) reveals that the main pattern of LCZ was still ZrO_2; however a few signature peaks of $LaCoO_3$ can be still observed in LCZ, confirming the presence of $LaCoO_3$ in LCZ. The surface chemistry of LCZ was also determined using XPS to reveal core-level spectra of major constituents (*i.e.*, La, Co, O and Zr) in LCZ. Fig. 3(a) shows two significant doublets located in the ranges of 830–840 eV and 847–857 eV, corresponding to La 3d₅/₂ and La 3d₃/₂. Specifically, the peaks at 833.6, 837.7, 850.5 and 854.6 eV all can be assigned to La^{3+}, validating that the valence state of La in $LaCoO_3$ is La^{3+} [26]. In the Co 2p
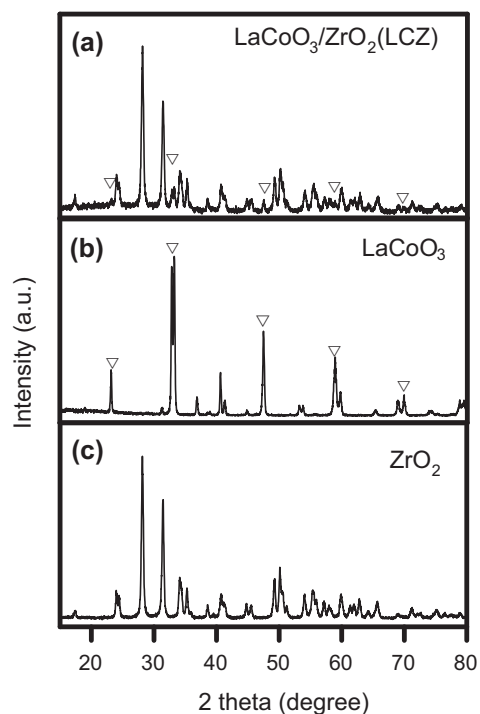
Fig. 2. XRD of (a) LaCoO₃/ZrO₂ (LCZ), (b) LaCoO₃, and (c) ZrO₂.

core-level spectrum (Fig. 3(b)), two noticeable peaks around 780 and 795 eV can be observed, corresponding to Co 2p₃/₂ and Co 2p₁/₂. These two peaks can be attributed to Co^{3+}, confirming the
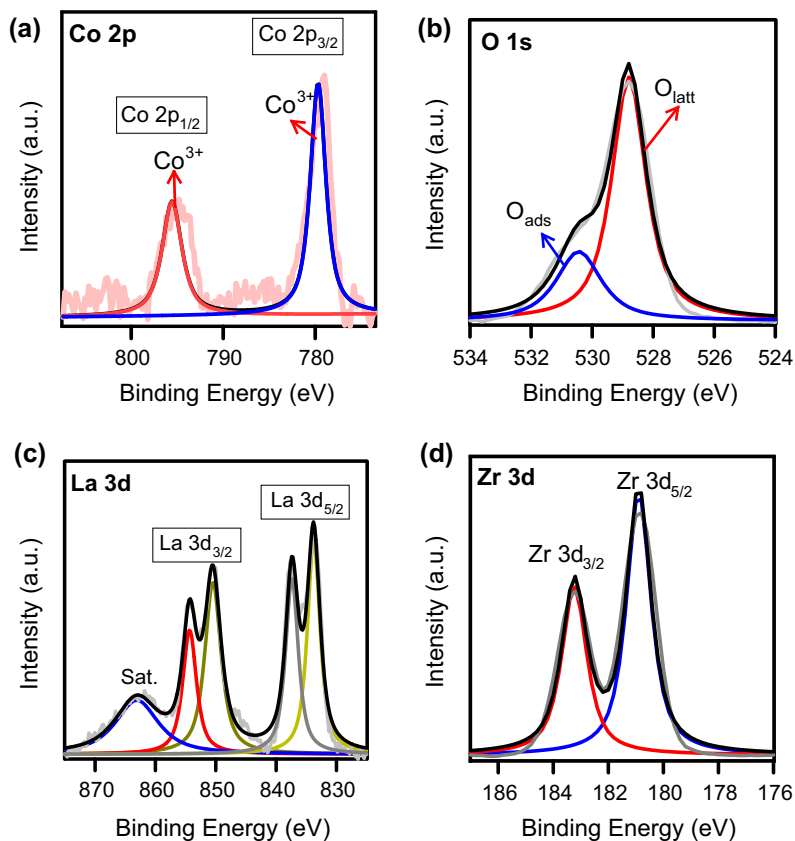
Fig. 3. XPS core-level spectra of LaCoO$_3$/ZrO$_2$(LCZ): (a) Co 2p, (b) O 1s, (c) La 3d and (d) Zr 3d.

valence state of Co^{3+} in LaCoO$_3$. On the other hand, Fig. 3(c) shows O 1s core-level spectrum, in which two peaks located at 528.8 eV and 530.4 eV, derived from the surface lattice oxygen (O$_{latt}$) and the surface adsorbed oxygen (O$_{ads}$), respectively [19]. The Zr 3d core-level spectrum can be seen in Fig. 3(d); two significant peaks can be detected at 181.6 and 183.9 eV, both corresponding to Zr^{4+} in ZrO$_2$, validating the formation of ZrO$_2$.

### 3.2. Roles of LCZ and Oxone in RB decolorization

Before evaluating catalytic activity of LCZ for activating Oxone, it is necessary to reveal whether RB could be decolorized via adsorption to LCZ. Fig. 4(a) shows that almost no RB was decolorized in the presence of LCZ, indicating that LCZ did not exhibit affinities toward RB in water. Fig. 4(a) also displays RB decolorization in the presence of Oxone alone. While RB was indeed decolorized, C_t/C_0 merely approached 0.75 after 60 min, demonstrating that Oxone without activation by catalysts could not generate sufficient sulfate radicals to decolorize RB. Nevertheless, once LCZ was combined with Oxone, RB was decolorized rapidly and C_t/C_0 reached zero at 60 min. As LCZ and Oxone were incapable of decolorizing RB individually, this result suggests that LCZ can activate Oxone and generate sulfate radicals efficiently. Fig. 4(a) also shows RB decolorization by LaCoO$_3$-activated Oxone, which was able to activate RB as C_t/C_0 also reached zero at 60 min. However, the decolorization kinetics obtained using LCZ is faster than that obtained using LaCoO$_3$, revealing that LCZ is more advantageous than bulk LaCoO$_3$ powder. Especially, as LCZ consisted of only 12.5 wt% of LaCoO$_3$, LCZ appears to be a promising and highly-efficient catalyst for activating Oxone, possibly owing to its relatively high surface compared that of bulk LaCoO$_3$. To further quan-

titatively compare decolorization kinetics, the pseudo first order rate law is adopted to analyze the kinetics as follows (Eq. (1)):

$$C_t = C_0 \exp(-k_1 t) \tag{1}$$

where k_1 is the pseudo first order rate constant. k_1 value obtained using LaCoO$_3$-activated Oxone is 0.060 min^{-1} (Table 1), whereas k_1 obtained using LCZ-activated Oxone is 0.171 min^{-1}, validating that LCZ is a much effective catalyst to activate Oxone than LaCoO$_3$.

To verify roles of LCZ catalyst and Oxone during RB decolorization, we further examined various concentrations of LCZ and Oxone. Fig. 4(b) displays RB decolorization using various concentrations of Oxone activated by a fixed amount of LCZ. At Oxone = 25 mg L^{-1}, the RB decolorization was quite limited as C_t/C_0 was not even below 0.6. Once Oxone increased to 50 mg L^{-1}, RB decolorization was substantially improved as C_t/C_0 approached 0.2. When Oxone concentration was further raised to 100 mg L^{-1}, RB was almost fully decolorized. The k_1 value also changed considerably from 0.009 to 0.171 min^{-1} as Oxone increased from 25 to 100 mg L^{-1}. These analyses indicate that a sufficient dosage of Oxone is required to generate enough sulfate radicals for rapid and complete decolorization. On the other hand, the concentration of LCZ was varied from 50 to 200 mg L^{-1}; the corresponding RB decolorization extents at equilibrium were interestingly comparable (Fig. 4(c)). This suggests that a relatively low amount of LCZ is needed to achieve full decolorization as LCZ plays a catalytic role during RB decolorization by Oxone. The k_1 value also increased from 0.109 to 0.350 min^{-1} as LCZ changed from 50 to 200 mg L^{-1}, validating the catalytic role of LCZ.
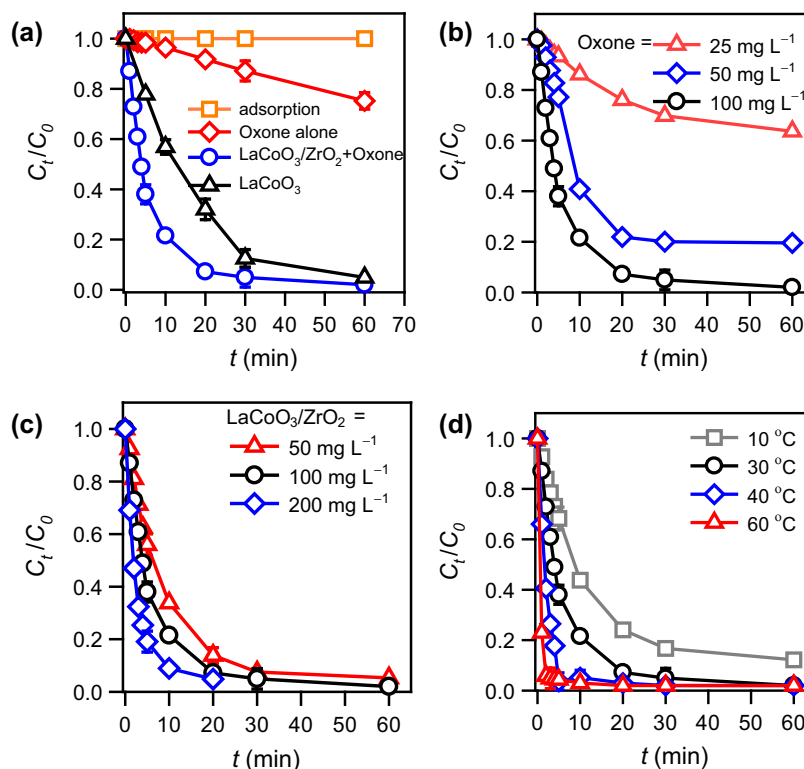
Fig. 4. Decolorization of RB by LCZ-activated Oxone: (a) comparison between adsorption to LCZ, Oxone alone, LCZ-activated Oxone and LaCoO$_3$-activated Oxone at 30 °C; (b) effect of LCZ loading at 30 °C; (c) effect of Oxone dosage at 30 °C; and (d) effect of temperature (RB = 10 mg L^{-1}, Oxone = 100 mg L^{-1}, LCZ = 100 mg L^{-1}).

Table 1
The pseudo first order rate constants of RB degradation by LaCoO$_3$/ZrO$_2$(LCZ)-activated Oxone under various conditions. (C_0 of RB = 10 mg L^{-1}).

Conditions					The pseudo first order rate constant	
LaCoO$_3$/ZrO$_2$ (LCZ) (mg L^{-1})	Oxone (mg L^{-1})	Temp. (°C)	pH	Additive	k_1 (min^{-1})	R^2
100 (LaCoO$_3$)	100	30	5	–	0.060	0.995
100	100	30	5	–	0.171	0.9926
200	100	30	5	–	0.350	0.990
50	100	30	5	–	0.109	0.994
100	25	30	5	–	0.009	0.921
100	50	30	5	–	0.069	0.950
100	100	10	5	–	0.070	0.982
100	100	40	5	–	0.457	0.991
100	100	60	5	–	1.427	0.992
100	100	30	3	–	0.042	0.996
100	100	30	7	–	0.029	0.989
100	100	30	9	–	0.011	0.994
100	100	30	11	–	0.001	0.720
100	100	30	5	NaF	0.172	0.990
100	100	30	5	NaCl	0.171	0.996
100	100	30	5	SDS	0.172	0.994
100	100	30	5	TBA	0.171	0.992
100	100	30	5	Methanol	0.021	0.964

3.3. Effects of temperature and pH on RB decolorization by LCZ-activated Oxone

To further investigate behaviors of Oxone activation by LCZ, RB decolorization was conducted at various conditions. First, solution temperature was changed to 10, 30, 40 and 60 °C to examine the effect of temperature. Fig. 4(d) shows that RB decolorization at 10 °C was not complete as C_t/C_0 reached merely 0.2. Nevertheless, C_t/C_0 can approach zero in 60 min when temperature increased to 30 °C, whereas it reached zero in 20 min at 40 °C and in 10 min at 60 °C. The k_1 values obtained at 10, 30, 40 and 60 °C are 0.071,

0.171, 0.457 and 1.427 min^{-1}, respectively. These results reveal that the increase in temperature not only influenced decolorization extent but also the degradation kinetics considerably. In view of faster decolorization kinetics at elevated temperatures, we further correlated rate constants to temperatures via the Arrhenius equation as follows (Eq.(2)):

$$\ln k_1 = \ln A - E_a/RT \tag{2}$$

where Ea represents the activation energy (E_a, kJ mol^{-1}); A denotes the pre-exponential factor (min^{-1}); R means the universal gas constant; and T denotes temperature (K). Based on Eq. (2), a plot of 1/T

vs ln k_1 of RB decolorization by LCZ-activated Oxone is displayed in Fig. S1 (see ESI†), in which the data points are well fit by linear regression with $R^2 = 0.975$. This evidences that rate constants of RB decolorization by LCZ-activated Oxone at various temperatures can be estimated by Arrhenius equation. The slope of the fitting line is then adopted to calculate the activation energies (Ea) as 47.8 kJ mol^{-1}.

Moreover, the RB decolorization was also evaluated at different pH to investigate LCZ-activated Oxone under acidic, neutral and alkaline conditions. Fig. 5(a) shows RB decolorization by LCZ-activated Oxone at pH = 3, 5, 7, 9 and 11, revealing that the effect of pH was significant on both decolorization extent and kinetics. As pH was 5 in the case of no pH adjustment, RB was almost fully decolorized at 60 min. Once pH became 3, the RB decolorization at equilibrium still approached zero at 60 min. Nevertheless, the decolorization kinetics was considerably slowed as k_1 changed from 0.171 to 0.042 min^{-1} when pH decreased from 5 to 3. This is because Oxone is much more stable under relatively acidic conditions, leading to slower activation of Oxone [27]. In contrast, once pH was increased from 5 to 7 by adding OH$^-$, the corresponding C_t/C_0, even though approaching zero at equilibrium, proceeded quite slowly with $k_1 = 0.0029$ min^{-1}. Catalytic activation of Oxone can be generally formulated as follows (Eq. (3))

$$HSO_5^- \overset{catalysts}{\rightarrow} CO^{3+} + SO_4^{\cdot-} + OH \qquad (3)$$

Thus, the presence of OH$^-$ could hinder the transformation of Oxone to sulfate radicals [27–29]. This adverse effect became even more pronounced at pH = 9 and 11 with $k_1 = 0.011$ and 0.001 min^{-1}, respectively. During the activation of Oxone, peroxymonosulfate anion (SO$_5^-$) is possibly converted to peroxymonosulfate radical (SO$_5^\cdot$), which can further evolve to sulfate radicals (SO$_4^\cdot$) as follows (Eq.(4)):

$$2SO_5^{\cdot-} \rightarrow 2SO_4^{\cdot-} + O_2 \qquad (4)$$

When a high concentration of OH$^-$ is present in RB solutions, OH$^-$ could be deposited on LCZ surface. Therefore, the approach of SO$_5^-$ to LCZ surface might be restrained, thereby diminishing the formation of SO$_4^-$ and leading to incompetent RB decolorization [30].

In addition, the variation of pH during the RB degradation by LCZ-activated Oxone under the typical experimental condition without adjustment of initial pH had been also measured (Fig. S2). The pH slightly and gradually decreased from 5 to 4.4 because of the resulting sulfate ions derived from Oxone activation. Even though pH was reduced because of sulfate ions, the variation of pH in fact remained quite similar over the curse of Oxone activation.

3.4. Effects of co-existing compounds and radical scavengers on RB decolorization by LCZ-activated Oxone

As Oxone is commonly adopted for degrading organic contaminants of wastewater, it is also essential to investigate how other co-existing compounds (e.g., salts and organic surfactants) present in wastewater affect activation of Oxone. NaCl was thus selected as a typical salt for evaluating its effect. Fig. 5(b) reveals that the presence of NaCl with an equivalent concentration as RB did not noticeably influenced RB decolorization on both decolorization extent and kinetics (i.e., k_1 remained as 0.171 min^{-1}). Even though a more reactive salt, NaF, was used, the RB decolorization remained almost the same ($k_1 = 0.172$). These results suggest that the presence of salts did not significantly affect activation of Oxone for RB decolorization. On the hand, as surfactants are easily present in wastewater, we selected SDS, an extensively-used anionic surfactant, for evaluating the effect of co-existing organics on Oxone activation. Nevertheless, the RB decolorization remained almost unchanged
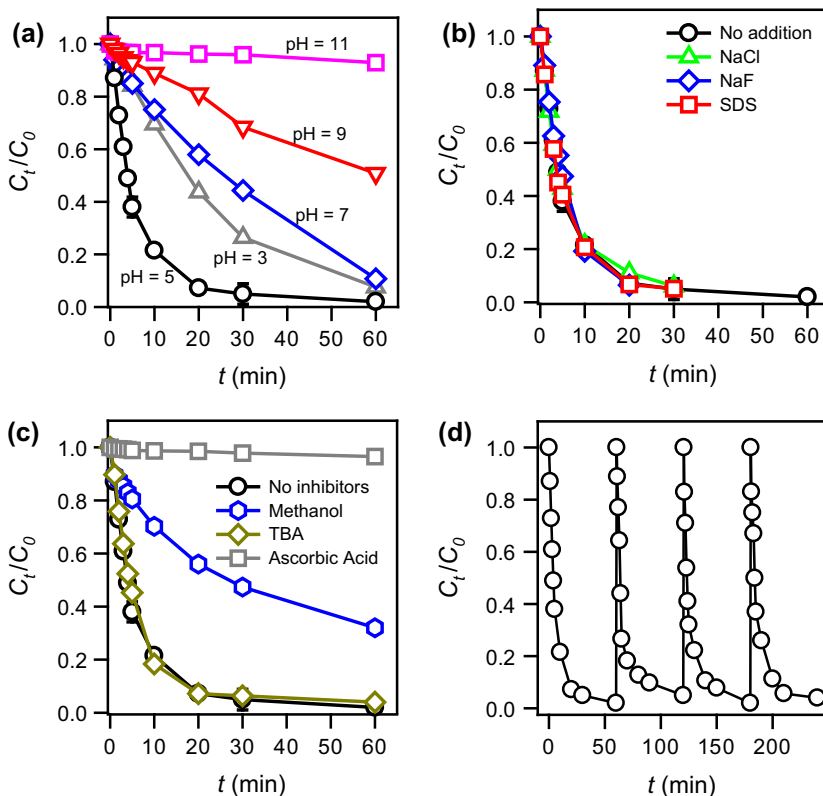

Fig. 5. Effects of (a) pH, (b) co-existing compounds and (c) inhibitors on decolorization of RB using LCZ–activated Oxone, (d) recyclability of LCZ–activated Oxone at 30 °C (RB = 10 mg L^{-1}, Oxone = 100 mg L^{-1}, LCZ = 100 mg L^{-1}).

even in the presence of SDS ($k_1 = 0.172$ min^{-1}), indicating that LCZ-activated Oxone remained effective even with other co-existing compounds.
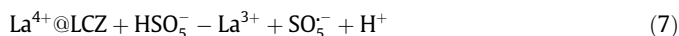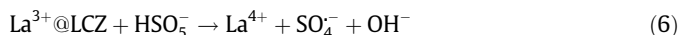
Moreover, specific radical scavengers were also evaluated for their inhibitive effects and for revealing the mechanism of RB decolorization by LCZ-activated Oxone. Ascorbic acid was first evaluated and added to RB solutions (Fig. 5(c)); the RB decolorization was completely inhibited. As ascorbic acid is a typical radical scavenger for reactive oxygen species, the complete inhibition indicates that RB indeed involved reactive oxygen species. In addition, since sulfate radicals can react with water to result in hydroxyl radicals (OH·) as follows [31] (Eq. (5)):

$$SO_4^{\cdot-} + H_2O \rightarrow SO_4^{2-} + OH^{\cdot} + H^+ \tag{5}$$
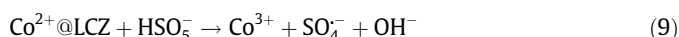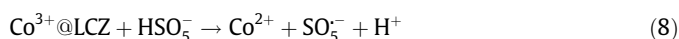
Therefore, it would be necessary to study whether OH· also participated in RB decolorization by LCZ-activated Oxone. To this end, TBA was particularly adopted as it is an OH·-specific scavenger. However, Fig. 5(c) reveals that RB decolorization by LCZ-activated Oxone in the presence of TBA was almost the same to that in the absence of any scavengers, demonstrating that the contribution of OH· for RB decolorization was insignificant. On the other hand, another radical scavenger, methanol, was further employed as it is a scavenger for both OH· and $SO_4^{\cdot-}$. Fig. 5(c) shows that the presence of methanol indeed inhibited RB decolorization substantially as C_t/C_0 merely approached 0.35 and k_1 decreased to 0.021 min^{-1}. Nevertheless, the inhibitive effect of methanol was as significant as that of ascorbic, indicating that other reactive oxygen species might be also involved. A previous study has reported that Oxone activation not only produces $SO_4^{\cdot-}$ but also induces the generation of $HO_2^{\cdot}$, $O_2^{\cdot}$, and $^1O_2$ [32]. Thus, these results of radical scavengers suggest that the RB degradation by LCZ-activated Oxone can be attributed to $SO_4^{\cdot-}$ as well as the induced reactive oxygen species (i.e., $HO_2^{\cdot}$, $O_2^{\cdot}$, and $^1O_2$).

3.5. The activation mechanism of LCZ to activate Oxone

In addition, we also studied the mechanism for activation of Oxone by LCZ. Since LCZ primarily consisted of La and Co, it is essential to distinguish which component plays a more important role for activating Oxone. As revealed in the XPS analysis, La ion in LCZ is La^{3+}. Thus, Oxone activation by La^{3+} was evaluated via RB decolorization. Fig. S3 shows that La^{3+}-activated Oxone was certainly more effective than Oxone alone, demonstrating the capability of La^{3+} for activating Oxone. La^{3+} might react with HSO$_5^-$ to generate sulfate radicals ($SO_4^{\cdot-}$) as follows (Eqs. (6) and (7)):

$$La^{3+}@LCZ + HSO_5^- \rightarrow La^{4+} + SO_4^{\cdot-} + OH^- \tag{6}$$

$$La^{4+}@LCZ + HSO_5^- - La^{3+} + SO_5^{\cdot-} + H^+ \tag{7}$$

However, the RB decolorization extent and kinetics were relatively low and slow, respectively compared to those by LCZ-activated Oxone. Thus, another constituent, Co^{3+}, might also contribute to activation of Oxone. Co^{3+} has been reported to react with Oxone to generate peroxymonosulfate (SO$_5$) and sulfate (SO$_4$) radicals through a series of reactions as follows (Eqs.(8) and (9)) [27,33–39]:

$$Co^{3+}@LCZ + HSO_5^- \rightarrow Co^{2+} + SO_5^{\cdot-} + H^+ \tag{8}$$

$$Co^{2+}@LCZ + HSO_5^- \rightarrow Co^{3+} + SO_4^{\cdot-} + OH^- \tag{9}$$

Therefore, the mechanism of Oxone activation by LCZ can be attributed to Co^{3+} and La^{3+} of LCZ.

Although LCZ is employed as a heterogeneous catalyst for Oxone activation, it is essential to investigate whether Oxone activation by LCZ involved with the leaching out of metals from LCZ. By measuring concentrations of La, Co, and Zr ions in the end of

RB degradation using LCZ-activated Oxone, we found that only a very small amount of La can be detected (0.09 mg L^{-1}); however the concentrations of Co and Zr were under detection limit. As we have shown in Fig. S3, La^{3+} (100 mg L^{-1}) was not highly efficient for activating Oxone, we found that 0.09 mg L^{-1} of La^{3+} could not activate Oxone. Thus, these results validate that the RB degradation by LCZ-activated Oxone was mainly attributed to a heterogeneous reaction.

3.6. The recyclability of LCZ to activate Oxone

Since LCZ is developed as a heterogeneous catalyst for activation of Oxone, LCZ must be reused for multiple times without loss of catalytic activity. Fig. 5(d) reveals that LCZ can be re-used without significant loss of catalytic activity over multiple cycles, demonstrating that LCZ can be a durable and recyclable heterogeneous catalyst for Oxone activation.

4. Conclusion

In this study, a zirconia-supported LaCoO$_3$ was particularly prepared as a heterogeneous catalyst for activating Oxone. In contrast to the low surface areas of bulk LaCoO$_3$ powder, the resulting LaCoO$_3$/ZrO$_2$ (LCZ) exhibited a significantly higher surface area (i.e., 10 times) than that of bulk LaCoO$_3$ powder. As RB decolorization was selected as a model test for evaluating catalytic activity of LCZ for activating Oxone, LCZ exhibited a much higher catalytic activity than LaCoO$_3$ for activating Oxone to decolorize RB. LCZ-activated Oxone also remained effective for RB decolorization even in the presence of salts and other organic contaminant. The mechanisms of RB decolorization by LCZ-activated Oxone were revealed and involved sulfate radical and other reactive oxygen species. The mechanism of Oxone activation by LCZ could be owing to both La^{3+} and Co^{3+} of LCZ. LCZ was recycled to activate Oxone for RB decolorization over multiple times without loss of catalytic activity. These findings demonstrate that LCZ is a promising LaCoO$_3$-based nanocomposite as a heterogeneous catalyst for activating Oxone to degrade organic pollutants.

Appendix A. Supplementary data

Supplementary data associated with this article can be found, in the online version, at http://dx.doi.org/10.1016/j.jcis.2017.03.004.

References

[1] M.A. Oturan, J.-J. Aaron, Advanced oxidation processes in water/wastewater treatment: principles and applications. A review, Crit. Rev. Environ. Sci. Technol. 44 (2014) 2577–2641.
[2] Q. Liao, J. Sun, L. Gao, Degradation of phenol by heterogeneous Fenton reaction using multi-walled carbon nanotube supported Fe$_2$O$_3$ catalysts, Coll. Surf. A: Physicochem. Eng. Asp. 345 (2009) 95–100.
[3] P. Neta, R.E. Huie, A.B. Ross, Rate constants for reactions of inorganic radicals in aqueous solution, J. Phys. Chem. Ref. Data 17 (1988) 1027–1284.
[4] Q. Yang, H. Choi, S.R. Al-Abed, D.D. Dionysiou, Iron–cobalt mixed oxide nanocatalysts: heterogeneous peroxymonosulfate activation, cobalt leaching, and ferromagnetic properties for environmental applications, Appl. Catal. B 88 (2009) 462–469.
[5] P. Shao, X. Duan, J. Xu, J. Tian, W. Shi, S. Gao, M. Xu, F. Cui, S. Wang, Heterogeneous activation of peroxymonosulfate by amorphous boron for degradation of bisphenol S, J. Hazard. Mater. 322 (Part B) (2017) 532–539.
[6] X. Duan, H. Sun, Z. Ao, L. Zhou, G. Wang, S. Wang, Unveiling the active sites of graphene-catalyzed peroxymonosulfate activation, Carbon 107 (2016) 371–378.
[7] Y. Wang, Z. Ao, H. Sun, X. Duan, S. Wang, Activation of peroxymonosulfate by carbonaceous oxygen groups: experimental and density functional theory calculations, Appl. Catal. B: Environ. 198 (2016) 295–302.
[8] X. Duan, K. O'Donnell, H. Sun, Y. Wang, S. Wang, Sulfur and nitrogen co-doped graphene for metal-free catalytic oxidation reactions, Small (2015) 3036–3044.

[9] X. Duan, Z. Ao, H. Sun, S. Indrawirawan, Y. Wang, J. Kang, F. Liang, Z.H. Zhu, S. Wang, Nitrogen-doped graphene for generation and evolution of reactive radicals by metal-free catalysis, ACS Appl. Mater. Interf. 7 (2015) 4169–4178.

[10] G. Zhou, L. Zhou, H. Sun, H.M. Ang, M.O. Tadé, S. Wang, Carbon microspheres supported cobalt catalysts for phenol oxidation with peroxymonosulfate, Chem. Eng. Res. Des. 101 (2015) 15–21.

[11] Y. Feng, J. Liu, D. Wu, Z. Zhou, Y. Deng, T. Zhang, K. Shih, Efficient degradation of sulfamethazine with CuCo₂O₄ spinel nanocatalysts for peroxymonosulfate activation, Chem. Eng. J. 280 (2015) 514–524.

[12] F. Gong, L. Wang, D. Li, F. Zhou, Y. Yao, W. Lu, S. Huang, W. Chen, An effective heterogeneous iron-based catalyst to activate peroxymonosulfate for organic contaminants removal, Chem. Eng. J. 267 (2015) 102–110.

[13] W.-D. Oh, Z. Dong, T.-T. Lim, Generation of sulfate radical through heterogeneous catalysis for organic contaminants removal: current development, challenges and prospects, Appl. Catal. B 194 (2016) 169–201.

[14] O.P. Taran, A.B. Ayusheev, O.L. Ogorodnikova, I.P. Prosvirin, L.A. Isupova, V.N. Parmon, Perovskite-like catalysts LaBO₃ (B = Cu, Fe, Mn Co, Ni) for wet peroxide oxidation of phenol, Appl. Catal. B 180 (2016) 86–93.

[15] Z. Jia, X. Duan, W. Zhang, W. Wang, H. Sun, S. Wang, L.-C. Zhang, Ultra-sustainable Fe78Si9B13 metallic glass as a catalyst for activation of persulfate on methylene blue degradation under UV-Vis light, Scient. Rep. 6 (2016) 38520.

[16] F. Chi, B. Song, B. Yang, Y. Lv, S. Ran, Q. Huo, Activation of peroxymonosulfate by BiFeO₃ microspheres under visible light irradiation for decomposition of organic pollutants, RSC Adv. 5 (2015) 67412–67417.

[17] X. Pang, Y. Guo, Y. Zhang, B. Xu, F. Qi, LaCoO₃ perovskite oxide activation of peroxymonosulfate for aqueous 2-phenyl-5-sulfobenzimidazole degradation: effect of synthetic method and the reaction mechanism, Chem. Eng. J. 304 (2016) 897–907.

[18] C. Su, X. Duan, J. Miao, Y. Zhong, W. Zhou, S. Wang, Z. Shao, Mixed conducting perovskite materials as superior catalysts for fast aqueous-phase advanced oxidation: a mechanistic study, ACS Catal. 7 (2017) 388–397.

[19] G. Guo, K. Lian, L. Wang, F. Gu, D. Han, Z. Wang, High specific surface area LaMO₃ (M = Co, Mn) hollow spheres: synthesis, characterization and catalytic properties in methane combustion, RSC Adv. 4 (2014) 58699–58707.

[20] C. Cai, H. Zhang, X. Zhong, L. Hou, Ultrasound enhanced heterogeneous activation of peroxymonosulfate by a bimetallic Fe–Co/SBA-15 catalyst for the degradation of Orange II in water, J. Hazard. Mater. 283 (2015) 70–79.

[21] T. Yamaguchi, Application of ZrO₂ as a catalyst and a catalyst support, Catal. Today 20 (1994) 199–217.

[22] F. Hiroaki, M. Noritaka, M. Makoto, Pronounced catalytic activity of La₁₋ₓSrₓCoO₃ highly dispersed on ZrO₂ for complete oxidation of propane, Chem. Lett. 16 (1987) 2147–2150.

[23] A.L. Kustov, O.P. Tkachenko, L.M. Kustov, B.V. Romanovsky, Lanthanum cobaltite perovskite supported onto mesoporous zirconium dioxide: nature of active sites of VOC oxidation, Environ. Int. 37 (2011) 1053–1056.

[24] Y. Wang, X. Yang, L. Lu, X. Wang, Experimental study on preparation of LaMO₃ (M = Fe Co, Ni) nanocrystals and their catalytic activity, Thermochim. Acta 443 (2006) 225–230.

[25] M. Jafarpour, E. Rezapour, M. Ghahramaninezhad, A. Rezaeifard, A novel protocol for selective synthesis of monoclinic zirconia nanoparticles as a heterogeneous catalyst for condensation of 1,2-diamines with 1,2-dicarbonyl compounds, New J. Chem. 38 (2014) 676–682.

[26] S. Phokha, S. Pinitsoontorn, S. Maensiri, S. Rujirawat, Structure, optical and magnetic properties of LaFeO₃ nanoparticles prepared by polymerized complex method, J. Sol-Gel Sci. Technol. 71 (2014) 333–341.

[27] W. Guo, S. Su, C. Yi, Z. Ma, Degradation of antibiotics amoxicillin by Co₃O₄-catalyzed peroxymonosulfate system, Environ. Prog. Sustain. Energy 32 (2013) 193–197.

[28] A. Rastogi, S.R. Al-Abed, D.D. Dionysiou, Sulfate radical-based ferrous–peroxymonosulfate oxidative system for PCBs degradation in aqueous and sediment systems, Appl. Catal. B 85 (2009) 171–179.

[29] J. Sun, X. Li, J. Feng, X. Tian, Oxone/Co²⁺ oxidation as an advanced oxidation process: comparison with traditional Fenton oxidation for treatment of landfill leachate, Water Res. 43 (2009) 4363–4369.

[30] F. Qi, W. Chu, B. Xu, Modeling the heterogeneous peroxymonosulfate/Co-MCM41 process for the degradation of caffeine and the study of influence of cobalt sources, Chem. Eng. J. 235 (2014) 10–18.

[31] L.J. Xu, W. Chu, L. Gan, Environmental application of graphene-based CoFe₂O₄ as an activator of peroxymonosulfate for the degradation of a plasticizer, Chem. Eng. J. 263 (2015) 435–443.

[32] D. Dai, Z. Yang, Y. Yao, L. Chen, G. Jia, L. Luo, Highly efficient removal of organic contaminants based on peroxymonosulfate activation by iron phthalocyanine: mechanism and the bicarbonate ion enhancement effect, Catal. Sci. Technol. 7 (2017) 934–942.

[33] J. Safari, Z. Mansouri Kafroudi, Z. Zarnegar, Co₃O₄-decorated carbon nanotubes as a novel efficient catalyst in the selective oxidation of benzoins, Comp. Rend. Chim. 17 (2014) 958–963.

[34] S. Muhammad, E. Saputra, H. Sun, J.d.C. Izidoro, D.A. Fungaro, H.M. Ang, M.O. Tade, S. Wang, Coal fly ash supported Co₃O₄ catalysts for phenol degradation using peroxymonosulfate, RSC Adv. 2 (2012) 5645–5650.

[35] Y. Yao, Z. Yang, H. Sun, S. Wang, Hydrothermal synthesis of Co₃O₄–graphene for heterogeneous activation of peroxymonosulfate for decomposition of phenol, Ind. Eng. Chem. Res. 51 (2012) 14958–14965.

[36] J. Shao, Z. Wan, H. Liu, H. Zheng, T. Gao, M. Shen, Q. Qu, H. Zheng, Metal organic frameworks-derived Co₃O₄ hollow dodecahedrons with controllable interiors as outstanding anodes for Li storage, J. Mater. Chem. A 2 (2014) 12194–12200.

[37] G. Zhang, C. Li, J. Liu, L. Zhou, R. Liu, X. Han, H. Huang, H. Hu, Y. Liu, Z. Kang, One-step conversion from metal-organic frameworks to Co₃O₄@N-doped carbon nanocomposites towards highly efficient oxygen reduction catalysts, J. Mater. Chem. A 2 (2014) 8184–8189.

[38] P. Shi, S. Zhu, H. Zheng, D. Li, S. Xu, Supported Co₃O₄ on expanded graphite as a catalyst for the degradation of Orange II in water using sulfate radicals, Desalin. Water Treat. 52 (2013) 3384–3391.

[39] F. Ghanbari, M. Moradi, M. Manshouri, Textile wastewater decolorization by zero valent iron activated peroxymonosulfate: compared with zero valent copper, J. Environ. Chem. Eng. 2 (2014) 1846–1851.